

The Calculation of NMR Chemical Shifts in Periodic Systems Based on Gauge Including Atomic Orbitals and Density Functional Theory

Dmitry Skachkov, Mykhaylo Krykunov, Eugene Kadantsev, and Tom Ziegler*

Department of Chemistry, University of Calgary, Calgary, Alberta, Canada T2N 1N4

Received January 22, 2010

Abstract: We present here a method that can calculate NMR shielding tensors from first principles for systems with translational invariance. Our approach is based on Kohn–Sham density functional theory and gauge-including atomic orbitals. Our scheme determines the shielding tensor as the second derivative of the total electronic energy with respect to an external magnetic field and a nuclear magnetic moment. The induced current density due to a periodic perturbation from nuclear magnetic moments is obtained through numerical differentiation, whereas the influence of the responding perturbation in terms of the external magnetic field is evaluated analytically. The method is implemented into the periodic program BAND. It employs a Bloch basis set made up of Slater-type or numeric atomic orbitals and represents the Kohn–Sham potential fully without the use of effective core potentials. Results from calculations of NMR shielding constants based on the present approach are presented for isolated molecules as well as systems with one-, two- and three-dimensional periodicity. The reported values are compared to experiment and results from calculations on cluster models.

1. Introduction

NMR shielding tensors can convey very important information about the local electronic structure around a nucleus in a periodic solid. It is thus not surprising that solid-state NMR is an active field of experimental research. This area has in recent years been supplemented with a number of computational schemes that are able to evaluate NMR shielding tensors from first principle.^{1–6} All these methods determine the shielding tensor as the second derivative of the total electronic energy with respect to an external magnetic field and a nuclear magnetic moment in one of two ways. In the first approach, the external magnetic field is considered as the initial perturbation inducing a current density and the nuclear magnetic dipole as the second perturbation responding to the induced current density. This is the order for the perturbations adopted in molecular NMR calculations as well as a recent periodic gauge-including projector augmented-wave (GIPAW) method developed by Mauri et al.^{2,3} in which the external magnetic field is further considered as oscillating in order to adopt to the periodic symmetry of the solid. In

the second converse approach, the order of the two perturbations is interchanged so that now the current density is induced by magnetic dipoles, whereas the external magnetic field is the responding perturbation. The converse approach has been pioneered by Thonhauser et al.^{4,5} in conjunction with GIPAW corrections and supercell techniques. It has the merit for solids that the first perturbation, due to the magnetic dipoles, can be considered periodic. However, special care must still be exercised in connection with the constant and nonperiodic external magnetic field. Sebastiani and coauthors⁶ applied an infinitesimal magnetic field and employed localized Wannier orbitals constructed from plane waves with continuous set of gauge transformations (CSGT) gauge corrections.⁷ In order to obtain sufficiently localized Wannier functions, Sebastiani too employed a supercell technique. All three implementations mentioned above make use of pseudo-potentials and plane waves.

The objective of this work is to develop a method for calculating the NMR chemical shift in periodic systems within the full potential program BAND^{8–11} in which use is made of atom-centered basis functions. Some of the magnetic properties (EPR g- and A-tensors) have already

* Corresponding author e-mail: ziegler@ucalgary.ca.

been implemented in BAND.^{12,13} In BAND the Bloch basis set is constructed from Slater-type orbitals (STOs) and/or numeric atomic orbitals (NAOs). The electronic density matrix near the nuclei is very important for NMR shielding and both STOs and NAOs afford a potentially accurate description of the Kohn–Sham (KS) orbitals in this region. Atomic centered basis functions allow for further use of gauge-included atomic orbitals (GIAOs) to ensure gauge invariant results.

We introduce in Section 2 a method for calculating the NMR chemical shift in periodic systems based on atom-centered basis functions with the computational details characteristic for BAND discussed in Section 3. We have tested our implementation on single molecules, diatomic chains as well as one-dimensional (1D) polymers, two-dimensional (2D) sheets, and a three-dimensional (3D) crystal of diamond. Our results are discussed in Section 4, where we make comparisons to experiment and other computational methods.

2. NMR Shielding Tensor in Periodic Systems

The NMR shielding tensor $\hat{\sigma}^N$ for nucleus N is defined as the second derivative of the total electronic energy with respect to an external magnetic field \mathbf{B} and a nuclear magnetic moment $\boldsymbol{\mu}_N$. For a periodic system, the NMR shielding tensor is the second derivative of the total electronic energy per unit cell:

$$\sigma_{\alpha\beta}^N = \left. \frac{\partial^2 E(\mathbf{B}, \boldsymbol{\mu}_N)}{\partial \mu_{N\alpha} \partial B_\beta} \right|_{\mathbf{B}=0, \boldsymbol{\mu}_N=0} \quad (1)$$

where $\mu_{N\alpha}$ and B_β are Cartesian components of the magnetic moment $\boldsymbol{\mu}_N$ and the magnetic field \mathbf{B} , respectively.

We shall use Kohn–Sham density functional theory¹⁴ (DFT) in this work. The total energy is given in DFT as a functional of the electronic density. The density, in turn, is represented as a sum of the auxiliary Kohn–Sham orbitals, Ψ_i :

$$\rho(\mathbf{k}, \mathbf{r}) = \sum_i n_i \Psi_i^*(\mathbf{k}, \mathbf{r}) \Psi_i(\mathbf{k}, \mathbf{r}) \quad (2)$$

here n_i is the occupation numbers for the KS orbitals, and the summation is over occupied orbitals. These orbitals are obtained as the self-consistent solution to the set of equations:

$$\mathbf{H} \Psi_i = \varepsilon_i \Psi_i \quad (3)$$

where the Hamiltonian has the form:

$$\mathbf{H} = \frac{1}{2} \mathbf{p}^2 + V^{\text{KS}}, \quad V^{\text{KS}} = V_{\text{XC}} + V_{\text{NUC}} + V_{\text{C}} \quad (4)$$

and \mathbf{p} is the momentum operator ($\mathbf{p} = -i\nabla$), V^{KS} is the effective Kohn–Sham potential, which is made up of an exchange–correlation potential accounting for many-body effects V_{XC} , an attractive potential due to nuclei V_{NUC} , and a classical electron repulsion potential V_{C} . Finally, Ψ_i and ε_i are an one electron Kohn–Sham orbital and an eigenvalue to (3), respectively.

The magnetic field is introduced into the Hamiltonian using the “minimum-coupling ansatz,”¹⁵ where a magnetic vector potential is added to the momentum operator:

$$\mathbf{p} \rightarrow \mathbf{p} + \frac{\mathbf{A}}{c} \quad (5)$$

By making use of eqs 4 and 5, the full Hamiltonian for the system can be written in the form:

$$\mathbf{H} = \mathbf{H}^0 + \frac{1}{c} \mathbf{A} \mathbf{p} + \frac{1}{2c^2} \mathbf{A}^2, \quad \mathbf{H}^0 = \frac{1}{2} \mathbf{p}^2 + V^{\text{KS}} \quad (6)$$

where \mathbf{A} is a vector potential. In NMR spectroscopy, the vector potential \mathbf{A} is made up of contributions from an external magnetic field and from nuclear magnetic moments, respectively:

$$\mathbf{A} = \mathbf{A}^{(\mu_N)} + \mathbf{A}^{(\mathbf{B})} \quad (7)$$

where $\mathbf{A}^{(\mathbf{B})}$ is a magnetic vector potential due to a constant external magnetic field \mathbf{B} that takes the form

$$\mathbf{A}^{(\mathbf{B})} = \frac{1}{2} [\mathbf{B} \times \mathbf{r}] \quad (8)$$

whereas $\mathbf{A}^{(\mu_N)}$ is a magnetic vector potential due to the magnetic dipoles and given by

$$\mathbf{A}^{(\mu_N)}(\mathbf{r}) = \sum_{\mathbf{T}} \frac{[\boldsymbol{\mu}_N \times \mathbf{r}_{NT}]}{|\mathbf{r}_{NT}|^3} \quad (9)$$

where $\mathbf{r}_{NT} = \mathbf{r} - \mathbf{R}_N - \mathbf{T}$, \mathbf{R}_N is the position of a probe atom N , and \mathbf{T} is the crystal vector. The infinite sum of dipole contributions is conditionally convergent in the 3D case and can be properly defined via analytic continuation techniques.¹⁶

Keeping in eq 6 terms containing the vector potentials to first order in $\mathbf{A}^{(\mu_N)}$ and $\mathbf{A}^{(\mathbf{B})}$ affords:

$$\mathbf{H} \approx \mathbf{H}^0 + \frac{1}{c} \mathbf{A}^{(\mu_N)} \mathbf{p} + \frac{1}{c} \mathbf{A}^{(\mathbf{B})} \mathbf{p} + \frac{1}{c^2} \mathbf{A}^{(\mu_N)} \mathbf{A}^{(\mathbf{B})} \quad (10)$$

In order to obtain solutions to eq 3 for periodic systems, the Kohn–Sham orbitals are expanded in terms of a complex Bloch basis set $\varphi_{\mu\mathbf{k}}$:¹⁶

$$\Psi_i(\mathbf{k}, \mathbf{r}) = \sum_{\mu} c_{\mu i \mathbf{k}} \varphi_{\mu\mathbf{k}}(\mathbf{r}) \quad (11)$$

where $\varphi_{\mu\mathbf{k}}$ is calculated as a Bloch sum of equivalent atomic orbitals $\varphi_{\mu}(\mathbf{r} - \mathbf{R}_{\mu} - \mathbf{T})$ separated by the crystal vector and centered on $\mathbf{R}_{\mu} + \mathbf{T}$:

$$\varphi_{\mu\mathbf{k}}(\mathbf{r}) \equiv \varphi_{\mu\mathbf{k}}(\mathbf{r} - \mathbf{R}_{\mu}) = \sum_{\mathbf{T}} \varphi_{\mu}(\mathbf{r} - \mathbf{R}_{\mu} - \mathbf{T}) e^{i\mathbf{k} \cdot \mathbf{T}} \quad (12)$$

To avoid gauge problems due to the use of a finite atomic basis set, we employ gauge-including atomic orbitals.¹⁷

In this case the Bloch basis set $\varphi_{\mu\mathbf{k}}$ depends on the magnetic field \mathbf{B} :

$$\varphi_{\mu\mathbf{k}}(\mathbf{r})^{\text{GIAO}} = \varphi_{\mu\mathbf{k}}(\mathbf{r}) e^{-i/2c(\mathbf{B} \times \mathbf{R}_{\mu}) \cdot \mathbf{r}} \quad (13)$$

In order to calculate the second derivative of the total electronic energy, we follow the procedure due to Gauss¹⁸ and write the expression for the energy Lagrangian with the usual orthonormality constraint:

$$\begin{aligned} \tilde{E} = & \int d\mathbf{k} \sum_i n_i \langle \Psi_i(\mathbf{k}, \mathbf{r}) | \mathbf{h} | \Psi_i(\mathbf{k}, \mathbf{r}) \rangle + \\ & \frac{1}{2} \int d\mathbf{k} \sum_i n_i \langle \Psi_i(\mathbf{k}, \mathbf{r}) | V_C | \Psi_i(\mathbf{k}, \mathbf{r}) \rangle + E_{XC}[\rho] - \\ & \int d\mathbf{k} \sum_i \varepsilon_{ij} n_i (\langle \Psi_i(\mathbf{k}, \mathbf{r}) | \Psi_j(\mathbf{k}, \mathbf{r}) \rangle - \delta_{ij}) \end{aligned} \quad (14)$$

Here the integration over \mathbf{k} -space is introduced, E_{XC} is the exchange–correlation energy,¹⁹ and \mathbf{h} contains the sum of the operators for the electronic kinetic energy and the electron nuclear attraction plus the magnetic vector potentials:

$$\mathbf{h} = -\frac{\nabla^2}{2} + V_{\text{NUC}} + \frac{1}{c} \mathbf{A}^{(\mu_N)} \mathbf{p} + \frac{1}{c} \mathbf{A}^{(\mathbf{B})} \mathbf{p} + \frac{1}{c^2} \mathbf{A}^{(\mu_N)} \mathbf{A}^{(\mathbf{B})}$$

For the second derivative we have the following expression:^{18,20}

$$\begin{aligned} \frac{d^2 \tilde{E}}{d\mathbf{B} d\boldsymbol{\mu}_N} = & \int d\mathbf{k} \left\{ \sum_{\mu\nu} P_{\mu\nu} \frac{\partial^2 h_{\mu\nu}}{\partial \mathbf{B} \partial \boldsymbol{\mu}_N} + \frac{\partial P_{\mu\nu}}{\partial \boldsymbol{\mu}_N} \frac{\partial h_{\mu\nu}}{\partial \mathbf{B}} + \frac{\partial P_{\mu\nu}}{\partial \boldsymbol{\mu}_N} \times \right. \\ & \left[\left\langle \frac{\partial \varphi_{\mu k}}{\partial \mathbf{B}} \right| V_C + V_{\text{XC}} \right| \varphi_{\nu k} \rangle + \left\langle \varphi_{\mu k} \right| V_C + V_{\text{XC}} \left| \frac{\partial \varphi_{\nu k}}{\partial \mathbf{B}} \right\rangle - \\ & \left. \frac{\partial W_{\mu\nu}}{\partial \boldsymbol{\mu}_N} \frac{\partial S_{\mu\nu}}{\partial \mathbf{B}} \right\} \end{aligned} \quad (15)$$

where we use the following definitions:

$$V_{\text{XC}} = \frac{\partial E_{\text{XC}}[\rho]}{\partial \rho} \text{ is the exchange–correlation potential}$$

$$P_{\mu\nu} = \sum_i n_i c_{\mu i}^* c_{\nu i} \text{ is the density } P \text{ matrix}$$

$$W_{\mu\nu} = \sum_i n_i c_{\mu i}^* \varepsilon_{ik} c_{\nu i} \text{ is the energy-weighted } P \text{ matrix}$$

$$S_{\mu\nu} = \langle \varphi_{\mu k} | \varphi_{\nu k} \rangle \text{ is the overlap matrix}$$

$$h_{\mu\nu} = \langle \varphi_{\mu k} | \mathbf{h} | \varphi_{\nu k} \rangle$$

The first term in eq 15 is the diamagnetic part of the shielding tensor; all other terms consist the paramagnetic shielding tensor. For the diamagnetic tensor, we have

$$\hat{\sigma}^{N,d} = \int d\mathbf{k} \sum_{\mu\nu} P_{\mu\nu} \frac{\partial^2 h_{\mu\nu}}{\partial \mathbf{B} \partial \boldsymbol{\mu}_N} \Big|_{\mathbf{B}=0, \boldsymbol{\mu}_N=0} \quad (16)$$

In order to evaluate $\hat{\sigma}^{N,d}$ of eq 16, use is made of the GIAO basis functions (eq 13) and the following expression for the derivatives of the GIAOs:

$$\frac{\partial \varphi_{\mu k}^{\text{GIAO}}}{\partial \mathbf{B}} = i \left[\frac{\mathbf{r}}{2c} \times \mathbf{R}_{\mu} \right] \varphi_{\mu k}^{\text{GIAO}} \quad (17)$$

By taking into account (eq 17) and employing the expression (eq 8) for $\mathbf{A}^{(\mathbf{B})}$, the diamagnetic tensor takes the final form:

$$\begin{aligned} \sigma_{\alpha\beta}^{N,d} = & \frac{1}{2c} \int d\mathbf{k} \sum_i n_i \sum_{\mu\nu} c_{\mu i}^{(0)*} c_{\nu i}^{(0)} \left\{ \left\langle \varphi_{\mu k} \right| \left[(\mathbf{r} - \mathbf{R}_{\nu}) \times \frac{1}{c} \frac{\partial \mathbf{A}^{(\mu_N)}}{\partial \mu_{N\alpha}} \right]_{\beta} \right| \varphi_{\nu k} \rangle + \\ & \left\langle \varphi_{\mu k} \right| [(\mathbf{r} - \mathbf{R}_{\nu}) \times (\mathbf{R}_{\nu} - \mathbf{R}_{\mu})]_{\beta} \frac{1}{c} \frac{\partial \mathbf{A}^{(\mu_N)}}{\partial \mu_{N\alpha}} \nabla \right| \varphi_{\nu k} \rangle \Big\} \end{aligned} \quad (18)$$

where the sum (eq 9) of $\mathbf{A}^{(\mu_N)}$ has only one atom from each cell and contains thus our probe atom N and its periodic images in other cells separated by the lattice vector \mathbf{T} . From expression (eq 18), we subtract a term

$$\frac{1}{2c} \int d\mathbf{k} \sum_i n_i \sum_{\mu\nu} c_{\mu i}^{(0)*} c_{\nu i}^{(0)} \left\langle \varphi_{\mu k} \right| [\mathbf{R}_{\nu} \times (\mathbf{R}_{\nu} - \mathbf{R}_{\mu})]_{\beta} \frac{1}{c} \frac{\partial \mathbf{A}^{(\mu_N)}}{\partial \mu_{N\alpha}} \nabla \right| \varphi_{\nu k} \rangle \quad (19)$$

to make the diamagnetic part invariant with respect to a displacement of the coordinate origin.

The paramagnetic shielding tensor can be written as

$$\begin{aligned} \hat{\sigma}^{N,p} = & \int d\mathbf{k} \left\{ \sum_{\mu\nu} \frac{\partial P_{\mu\nu}}{\partial \boldsymbol{\mu}_N} \frac{\partial h_{\mu\nu}}{\partial \mathbf{B}} + \frac{\partial P_{\mu\nu}}{\partial \boldsymbol{\mu}_N} \left[\left\langle \frac{\partial \varphi_{\mu k}}{\partial \mathbf{B}} \right| V_C + V_{\text{XC}} \right| \varphi_{\nu k} \rangle + \right. \\ & \left. \left\langle \varphi_{\mu k} \right| V_C + V_{\text{XC}} \left| \frac{\partial \varphi_{\nu k}}{\partial \mathbf{B}} \right\rangle \right] - \frac{\partial W_{\mu\nu}}{\partial \boldsymbol{\mu}_N} \frac{\partial S_{\mu\nu}}{\partial \mathbf{B}} \Big\} \Big|_{\mathbf{B}=0, \boldsymbol{\mu}_N=0} \end{aligned} \quad (20)$$

In order to calculate (eq 20), we use the expression:

$$\frac{\partial S_{\mu\nu}}{\partial \mathbf{B}} = i \left\langle \varphi_{\mu k}^{\text{GIAO}} \right| \left[\frac{\mathbf{r}}{2c} \times (\mathbf{R}_{\nu} - \mathbf{R}_{\mu}) \right] \left| \varphi_{\nu k}^{\text{GIAO}} \right\rangle \quad (21)$$

For the paramagnetic tensor, we apply analytic differentiation with respect to the external magnetic field components and the numerical differentiation with respect to the magnetic dipole moment components. We make use of numerical differentiation for the magnetic dipole moment to avoid²⁰ potential problems related to near degeneracies between occupied and virtual orbitals (for example, for 2D graphite).²¹ Such problems do not occur for the external magnetic field as it is the second and responding perturbation. Thus, use can be made of analytic differentiation in this case. The final formula for the paramagnetic tensor takes the form:

$$\begin{aligned} \sigma_{\alpha\beta}^{N,p} = & \frac{1}{2c} \int d\mathbf{k} \sum_i n_i \sum_{\mu\nu} (-i) \frac{\partial}{\partial \mu_{N\alpha}} (c_{\mu i}^{(\mu_N)*} c_{\nu i}^{(\mu_N)}) \left\{ \left\langle \varphi_{\mu k} \right| [(\mathbf{r} - \mathbf{R}_{\nu}) \times \right. \\ & \left. \nabla]_{\beta} | \varphi_{\nu k} \rangle + \langle \varphi_{\mu k} | [\mathbf{r} \times (\mathbf{R}_{\nu} - \mathbf{R}_{\mu})]_{\beta} (\mathbf{H}^0 - \varepsilon_{ik}^{(0)}) | \varphi_{\nu k} \rangle \right\} \end{aligned} \quad (22)$$

where $c_{\mu i}^{(\mu_N)}$ is the numerical solution for (eq 3) with only the perturbation by $\boldsymbol{\mu}_N$ included.

According to the recipe of Fukui,²² we add the term (eq 19) to the paramagnetic contribution in order to make both paramagnetic and diamagnetic terms individually origin invariant.

In order to evaluate the numerical derivative

$$\frac{\partial}{\partial \mu_{N\alpha}} (c_{\mu i}^{(\mu_N)*} c_{\nu i}^{(\mu_N)}) \quad (23)$$

with respect to the magnetic dipole moment component, we make use of the fact that there are identical magnetic dipole moments $\boldsymbol{\mu}_N$ from one equivalent atom N (see Figure 1) in each cell.

The Hamiltonian perturbed by a periodic distribution of nuclear dipole moments $\boldsymbol{\mu}_N$ has the form

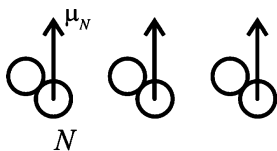


Figure 1. Magnetic dipole moments on equivalent atoms N .

$$\mathbf{H} = \mathbf{H}^0 + \frac{1}{c} \mathbf{A}^{(\mu_N)} \mathbf{p} \quad (24)$$

where the vector magnetic potential from the periodic distribution of dipoles μ_N has a form given in eq 9.

We stress again that $\mathbf{A}^{(\mu_N)}$ is a sum made up of a single contribution from one magnetic dipole moment in each cell. The KS equation with the perturbed Hamiltonian (eq 24) are solved separately for μ_{Nx} , μ_{Ny} , and μ_{Nz} , respectively. We have found a single point numerical differentiation with displacements $\Delta\mu_{N\alpha} = 0.01$ au to be numerically stable.

Since the Bloch basis set is complex, the first-order change in density with respect to a magnetic field

$$\left. \frac{\partial \rho(\mathbf{k}, \mathbf{r})}{\partial B_\beta} \right|_{B_\beta=0} = \frac{1}{2c} \sum_i n_i \sum_{\mu\nu} c_{\mu ik}^{(0)*} c_{\nu ik}^{(0)} \varphi_{\mu k}^* [\mathbf{r} \times (\mathbf{R}_\nu - \mathbf{R}_\mu)]_\beta \varphi_{\nu k} \quad (25)$$

is not equal to zero in each \mathbf{k} point. However, the first-order change in density in \mathbf{k} will be canceled by the corresponding change in $-\mathbf{k}$. It can be shown based on the fact that for Bloch functions in a $-\mathbf{k}$ point we have

$$\varphi_{\mu, -\mathbf{k}} = \varphi_{\mu k}^* \quad (26)$$

according to (eq 12). Further, $c_{\mu, -\mathbf{k}}^{(0)} = c_{\mu k}^{(0)*}$ in order to keep properties of the Bloch functions (eq 11) (time-reversal symmetry).²³ Thus we have

$$\left. \frac{\partial \rho(\mathbf{k}, \mathbf{r})}{\partial B_\beta} \right|_{B_\beta=0} = - \left. \frac{\partial \rho(-\mathbf{k}, \mathbf{r})}{\partial B_\beta} \right|_{B_\beta=0}$$

Therefore, the calculation of NMR shielding tensors of periodic systems is based on uncoupled perturbation theory²⁴ as in the case of single molecules, since the total first-order changes in the density in both types of systems are zero.

In evaluating $\hat{\sigma}^{N,d}$ of eq 18 and $\hat{\sigma}^{N,p}$ of eq 22, the integration is over a single unit cell. However, the unit cell must be large enough so that the current density induced by the magnetic moment of the single probe atom N in that cell is practically falling off to zero at the borders of that cell. If this condition is satisfied, then it does not matter that the operator due to the magnetic field is not periodic. This is so since our assumption about the induced current density in conjunction with the use of GIAOs will ensure that integration over any unit cell to obtain $\hat{\sigma}^{N,d}$ and $\hat{\sigma}^{N,p}$ will give the same results. Thus, in order to calculate $\hat{\sigma}^{N,d}$ and $\hat{\sigma}^{N,p}$ in some cell \mathbf{T}_0 , we need to change $\mathbf{r} \rightarrow \mathbf{r} + \mathbf{T}_0$ and $\mathbf{R}_\mu \rightarrow \mathbf{R}_\mu + \mathbf{T}_0$, and this does not change the diamagnetic tensor value since $\hat{\sigma}^{N,d}$ has only $\mathbf{r} - \mathbf{R}_\mu$ and $\mathbf{R}_\nu - \mathbf{R}_\mu$ terms. Moreover, integration in the cell \mathbf{T}_0 is equivalent to origin shift by \mathbf{T}_0 , and we have already discussed the origin invariance of paramagnetic tensor.

The problem of the operator representing the interaction between the electrons and the external magnetic field is not periodic has been treated in different ways by various authors.^{25–27} Following the original suggestion by Thornhauser et al.,²⁶ we consider the magnetic dipole as the first perturbation in what the authors have termed a converse approach, since the external magnetic field traditionally has been considered as the first perturbation. In the converse approach, one can use periodicity of the perturbing potential. However, such an approach does not completely circumvent the problem of the nonperiodic operator due to the external magnetic field.

To incorporate this aspect it is important to note that the shielding constant for nuclei N , as defined in eq 1, is related to the interaction energy $\Delta E_{\alpha\beta}$ between the current density ΔJ_α induced by the nuclear magnetic moment component $\mu_{N,\alpha}$ on N and the external magnetic field component B_β by $\Delta E_{\alpha\beta} = \sigma_{\alpha\beta}^N \mu_{N,\alpha} B_\beta$. The induced current density ΔJ_α from nuclei N is not periodic. However, we can assume that it vanishes outside the border of some region (supercell). Thus $\Delta E_{\alpha\beta}$ and $\sigma_{\alpha\beta}^N$ can be evaluated by integration within this supercell. It is implicit in the definition of $\sigma_{\alpha\beta}^N$ that only contributions from the current density of nucleus N (and not its periodic images) shall be considered in evaluating $\sigma_{\alpha\beta}^N$. Note, we can still operate with a periodic magnetic vector potential $\mathbf{A}^{(\mu_N)}$ as long as the magnetic moment due to $\mu_{N,\alpha}$ vanishes outside the border of the supercell to which N belongs.

3. Computational Details

The Bloch states are expanded in a mixed basis of Slater-type and numerical atomic orbitals with the radial part of each NAO stored on a grid. Such a basis is well suited for an accurate representation of the electron density near the nuclei. Use was made of a triple- ζ basis consisting of two STOs and one NAO for each nl subshell (1s, 2s, 2p, etc.). This basis was augmented with two STO polarization functions. This basis is referred to as TZ2P in the BAND's basis set database. In some cases, a STO component from one or more nl subshells had to be removed in order to avoid linear dependencies. The numerical accuracy parameter used by BAND has been set to five. Most of the calculations are carried out with BAND's parameter *k*space equal to five and three. Here the *k*space parameter of the BAND program describes the number of integration points in each \mathbf{k} direction in reciprocal space. For odd *k*space values, BAND uses quadratic integration schemes for 1D, 2D,⁹ and 3D¹⁰ Brillouin zones.

In order to calculate the crystal orbitals perturbed by the nuclear dipole moments μ_N (coefficients $c_{\mu ik}^{(\mu_N)}$), we calculate the matrix elements

$$\left\langle \varphi_{\mu k} \left| \frac{1}{c} \mathbf{A}^{(\mu_N)} \mathbf{p} \right| \varphi_{\nu k} \right\rangle \quad (27)$$

involving the perturbing Hamiltonian (eq 24) and add them to the corresponding matrix elements containing the unperturbed Hamiltonian. The resulting matrix is subsequently diagonalized. Only one SCF cycle is required since the magnetic perturbation is purely imaginary. Thus, no first-

Table 1. Calculated Shielding Constants (in ppm) for Molecular Water in a Cubic Super-Cell Compared to Experiment and Molecular ADF Calculations

atom	BAND ^a		ADF	experiment ^b
	STOs basis set	mixed NAOs/STOs basis set		
O	331.21	329.36	331.71	344.0
H	31.79	31.82	31.79	30.1

^a Cubic supercell dimension $a = 30$ Å. ^b Experimental data from ref 35.

order change is induced in the density and the corresponding Coulomb and exchange–correlation potentials.

All calculations are based on spin restricted SCF calculations employing the generalized gradient approximation (GGA) for the exchange–correlation energy. The parametrization of the exchange–correlation energy follows that of Becke²⁸ for the exchange and Perdew^{29,30} for the correlation.

Since Bloch eigenstates are only defined within a phase factor, the solutions $c_{\mu k}^{(\mu_N)}$ and $c_{\mu k}^{(0)}$ may differ by a phase. In order to avoid this problem, use was made of the following expression for calculating the derivative (eq 23):

$$\frac{\partial}{\partial \mu_N} (c_{\mu k}^{(\mu_N)*} c_{\nu k}^{(\mu_N)}) \approx \frac{c_{\mu k}^{(\mu_N)*} c_{\nu k}^{(\mu_N)} - c_{\mu k}^{(0)*} c_{\nu k}^{(0)}}{|\mu_N|} \quad (28)$$

instead of a direct numerical differentiation of the solutions $c_{\mu k}^{(\mu_N)}$.

Only time-reversal symmetry is used in integration over the Brillouin zone, since symmetry cannot be employed as the perturbation (eq 24) does not commute with the symmetry operations.

4. Results

We have tested our BAND implementation for the calculation of NMR shielding tensors by comparing our results with experiment, with calculations reported in the literature, and with calculations using the molecular ADF code.^{31–34}

Single Molecule of Water. The simplest test system for the calculation of NMR shielding by a periodic code is a single molecule in a big box. Calculations have been carried out on one water molecule in a large cubic supercell with $a = 30$ Å, employing two different basis sets and an experimental geometry. In the first case, we have employed a pure STO TZ2P basis from the ADF database without NAOs. In the second case, use was made of a mixed NAO/STO TZ2P basis from the database of BAND, as described in Section 3, Computational Details. The results are listed in the Table 1.

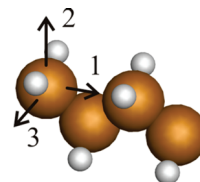
It is clear from Table 1 that BAND and ADF afford quite similar results for the same TZ2P basis consisting of STOs only. Employing a mixed TZ2P STO/NAO basis introduces only a minor change in the results obtained by BAND. Thus employing a pure STO or a mixed STO/NAO TZ2P basis in BAND is likely to afford results of similar accuracy compared to experimental results.

One-Dimensional Periodic Systems. In order to test our implementation on periodic systems, we have carried out a

Table 2. Shielding Constants for Chains of Diatomic Molecules

chain	period, Å	atom probed by NMR	isotropic shielding constant for molecular chains, ppm		isotropic shielding constant for single molecule, ppm
			BAND ^a	ADF ^b	
H ₂	2.38	H	19.59	19.53	22.17
F ₂	3.00	F	−181	−195	−258.7
HCl	2.70	H	20.5	20.1	31.9
		Cl	762	775	954

^a BAND calculations with $k_{space} = 5$ and 5 molecules in one supercell; TZ2P NAO/STO basis. ^b ADF calculations based on a cluster of 40 molecules; TZ2P STO basis.

**Figure 2.** Polyethylene cells and principal axis of the shielding tensor.

set of calculations for 1D systems. The systems consisted of diatomic chains and polymers.

Diatomic Chains. Calculated isotropic shielding constants for chains of H₂, F₂, and HCl molecules are listed in Table 2. All constants obtained by BAND were compared to results from ADF calculations on a cluster model consisting of 40 molecules.

We find in general for chains of diatomic molecules that a total number of five molecules are required in a unit cell to satisfy our boundary condition of diminishing induced current density at the edges. Thus, making use of only three molecules per cell changed the calculated constants by a few ppm. On the other hand, increasing the number of molecules to seven had only a marginal influence on the calculated constants ($\sim 0.1\%$). The calculated shielding constants had converged with the use of five \mathbf{k} points (BAND's parameter $k_{space} = 5$).

Polyethylene (PE) has two carbon and four hydrogen atoms in each primitive cell with a period of $T = 2.553$ Å (see Figure 2). The bond angles and lengths used in the calculation were taken from experimental X-ray data.^{36,37} For the C–H bond length, we adopted a value of $r_{CH} = 1.09$ Å.³⁷ The results for the principal and isotropic values of the chemical shift are listed in the Table 3. Also shown are experimental findings³⁸ along with ADF results from a calculation on a molecular cluster, CH₃–(CH₂)₁₆–CH₃. The induced paramagnetic current

$$\mathbf{J}^p(\mathbf{r}) = \int d\mathbf{k} \sum_i n_i \frac{1}{2c} \text{Im}(\Psi_i^{(\mu_N)*}(\mathbf{k}, \mathbf{r}) \nabla \Psi_i^{(\mu_N)}(\mathbf{k}, \mathbf{r}))$$

where $\Psi_i^{(\mu_N)}(\mathbf{k}, \mathbf{r})$ are the KS orbitals perturbed by the nuclear moment μ_N of our probing carbon atom, and its periodic image in the other supercells is shown in Figure 3 for polyethylene. Figure 3 depicts the paramagnetic current in one supercell consisting of three primitive cells of PE. The big circles show carbon atoms, the small circles show

Table 3. Carbon Chemical Shifts (in ppm) for Polyethylene with Respect to TMS^a

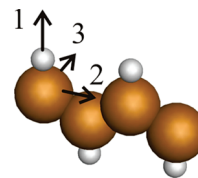
	BAND ^b	ADF cluster ^c	experiment ^d
δ_{11}	16.2	18.3	15.5
δ_{22}	36.6	48.8	33.9
δ_{33}	55.0	45.2	51.1
δ_{iso}	35.9	37.4	33.5

^a Tetramethylsilane. ^b BAND calculations with $k\text{space} = 3$ and 3 primitive cells as a supercell; TZ2P NAO/STO basis. ^c ADF calculations based on a $\text{CH}_3-(\text{CH}_2)_{16}-\text{CH}_3$ cluster, where the calculated shift corresponds to one of the two central carbons; TZ2P STO basis. ^d From ref 38.

hydrogen atoms. The intensity of color is proportional to the absolute value of the current. The paramagnetic current is located mostly on carbon atoms. It is almost zero on the hydrogens. It is clear from Figure 3 that using one primitive cell to calculate the paramagnetic shielding tensor is not enough and that we need to take into consideration the nearest cells. To reach convergence for the shielding tensor, we need to take three primitive cells as one big supercell and make integration in \mathbf{k} -space with three \mathbf{k} -points ($k\text{space} = 3$).

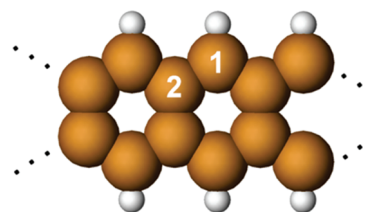
The chemical shift is calculated with respect to tetramethylsilane (TMS) as $\delta^{13\text{C}} = \sigma_{\text{TMS}}^{13\text{C}} - \sigma_{\text{PE}}^{13\text{C}}$, where the TMS isotropic shielding tensor is calculated by the ADF program. For the ADF cluster calculation on $\text{CH}_3-(\text{CH}_2)_8-\text{C}^*\text{H}_2-(\text{CH}_2)_7-\text{CH}_3$, we obtained a value of 37.4 ppm compared to the BAND result of 35.9 ppm and the experimental value of 33.5 ppm. Thus there seems to be good agreement between experiment and theory. It should, however, be pointed out that the experimental value corresponds to PE folded in 3D. Nevertheless the comparison is still valid since 3D PE “locally” can be considered linear.

Trans-polyacetylene (PA) has two atoms of carbon and two atoms of hydrogen in a primitive cell with a period of $T = 2.457 \text{ \AA}$ (Figure 4). The bond angles and lengths used in the calculation were taken from experimental X-ray data.³⁹ The result for the isotropic value of the chemical shift is listed in the Table 4. Also shown are experimental findings along with ADF results from a calculation on a molecular cluster, $\text{H}-(\text{CH})_{80}-\text{H}$. BAND result is 142.3 ppm, convergence is reached with a $k\text{space}$ parameter equal to 5 (total number of \mathbf{k} -points equal to 5) and 5 primitive cells as a

**Figure 4.** Trans-polyacetylene cells and principal axis of the shielding tensor.**Table 4.** Carbon Chemical Shift (in ppm) for Trans-PA with Respect to TMS

	BAND ^a	ADF cluster ^b	experiment ^c
δ_{11}	221.0	218.4	219
δ_{22}	155.1	140.1	144
δ_{33}	50.7	45.5	47
δ_{iso}	142.3	134.6	137.3

^a BAND calculations with $k\text{space} = 5$ and 5 primitive cells as a supercell; TZ2P NAO/STO basis. ^b ADF calculations based on a $\text{H}-(\text{CH})_{80}-\text{H}$ cluster with the central carbon as the NMR probe; TZ2P STO basis. ^c From ref 40.

**Figure 5.** Carbon nanoribbon.

supercell. For the ADF cluster, we have obtained a value for the shielding constant of 134.6 ppm. The experimental estimate is 137.3 ppm.

Carbon nanoribbon is a 1D polymer with four atoms of carbon and two atoms of hydrogen in a primitive cell (Figure 5). The C–C bond length used in the calculation is $r_{\text{CC}} = 1.418 \text{ \AA}$. The result for the isotropic value of the chemical shifts is listed in the Table 5. Also shown are calculated results by other authors along with ADF results from a calculation on a molecular cluster consisting of 44 benzene rings. BAND result is 138.4 and 147.1 ppm for two types of carbon atoms (see Figure 5). Convergence is reached with $k\text{space} = 5$ (total number of \mathbf{k} -points) and 5 primitive cells as a supercell. For the ADF cluster, we have obtained values

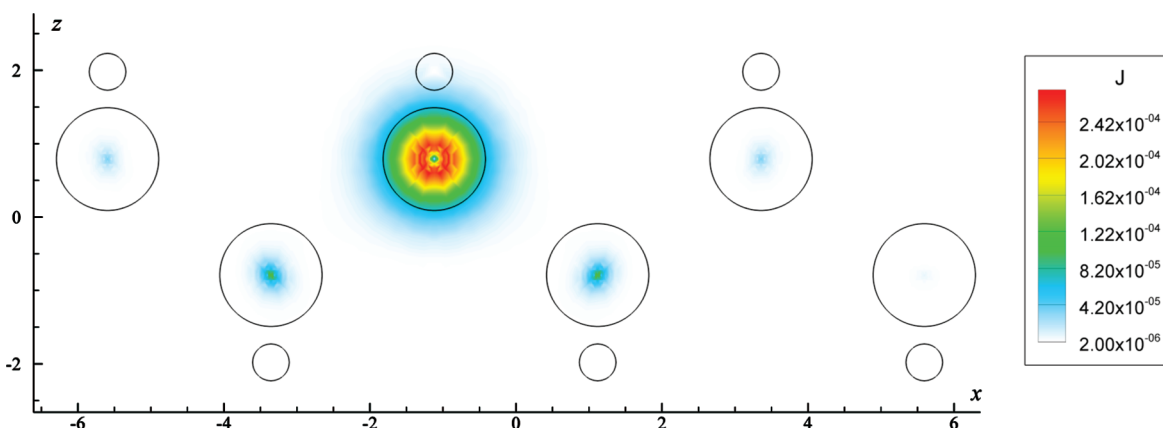
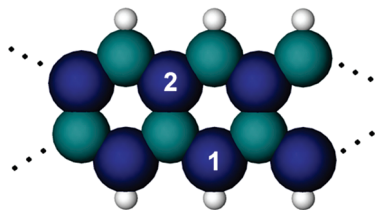
**Figure 3.** The paramagnetic current for polyethylene; x and z coordinates and absolute value of the current are in au.

Table 5. Carbon Chemical Shift (in ppm) for Carbon Nanoribbon with Respect to TMS

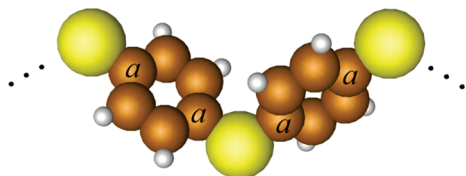
	atom probed by NMR	BAND ^a	ADF cluster ^b	calculated by other authors
carbon	C ₁	138.4	131.9	128.0 ^c
nanoribbon	C ₂	147.1	137.1	132.2 ^c

^a BAND calculations with *k*space = 5 and 5 primitive cells as a supercell; TZ2P NAO/STO basis. ^b ADF calculations based on a H₂-(C₄H₂)₄₃-C₂H₂ cluster with the central carbon as the NMR probe; TZ2P STO basis. ^c From ref 5.

**Figure 6.** Boron nitride nanoribbon.**Table 6.** Nitrogen Chemical Shift (in ppm) for a Boron Nitride Nanoribbon with Respect to CH₃-NO₂

	atom probed by NMR	BAND ^a	ADF cluster ^b
BN nanoribbon	N ₁	-261.1	-270.9
	N ₂	-220.6	-228.8

^a BAND calculations with *k*space = 3 and 5 primitive cells as a supercell; TZ2P NAO/STO basis. ^b ADF calculations based on a H₂-(B₂N₂H₂)₄₄-BN-H₂ cluster with the central carbon as the NMR probe; TZ2P STO basis.

**Figure 7.** Poly(*p*-phenylene sulfide) cell.

for the shielding constants of 131.9 and 137.1 ppm, respectively. The result by Thonhauser et al. is 128.0 and 132.2 ppm.

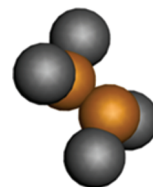
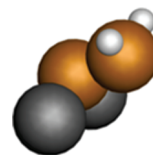
Boron nitride nanoribbon is a 1D polymer with two atoms each of boron, nitrogen, and hydrogen in a primitive cell (Figure 6). The B-N bond length used in the calculation is $r_{\text{BN}} = 1.446 \text{ \AA}$. The results for the nitrogen shielding shifts with respect to nitromethane are listed in the Table 6. Also shown are ADF results from a calculation on a molecular cluster consisting of 44 BN rings. BAND result is -261.1 ppm for the first atom and -220.6 ppm for the second. Convergence is reached with *k*space = 3 (3 **k**-points) and 5 primitive cells as a supercell. For the ADF cluster, we have obtained values for the shielding constants of -270.9 and -228.8 ppm, respectively.

Poly(*p*-phenylene sulfide) (PPS) cell consist of two atoms of sulfur, twelve atoms of carbon, and eight atoms of hydrogen (Figure 7) with period of 10.26 Å. The bond angles and lengths used in the calculation were taken from experimental data.^{41,42} There are two types of carbon atoms due to symmetry: type *a* (marked in Figure 7) and *b* (all other carbon atoms). The result for the isotropic value of the chemical shifts for two types of atoms is listed in the

Table 7. ¹³C Chemical Shift (in ppm) for PPS with Respect to TMS

	atom probed by NMR	BAND ^a	experiment ^b
PPS	C _a	134.8	135.1
	C _b	131.1	131.8

^a BAND calculations with *k*space = 3 and one primitive cell; TZ2P NAO/STO basis. ^b From refs 43 and 44.

**Figure 8.** Teflon cell.**Figure 9.** PVDF cell.**Table 8.** ¹⁹F Chemical Shifts (in ppm) for PVDF^a and Teflon^b

polymer	atom probed by NMR	BAND	ADF cluster	experiment
PVDF	F	-135.0 ^c	-133.9 ^d	91.6, 94.8, 113.6, 115.6 ^f
teflon	F	-585.8 ^c	-588.1 ^e	-549 ^g

^a With respect to CFCI₃. ^b With respect to F₂. ^c BAND calculations with *k*space = 3 and 3 primitive cells as a supercell; TZ2P NAO/STO basis. ^d ADF calculations based on a CH₃-(CF₂-CH₂)₁₉-H cluster; TZ2P STO basis. ^e ADF calculations based on a F-(CF₂)₂₈-F cluster; TZ2P STO basis. ^f From ref 47. ^g From ref 48.

Table 7. Calculations have shown that to reach convergence for such a big system one primitive cell is enough. The results calculated in BAND are very closed to the experimental values.

Polytetrafluoroethylene (PTFE). The PTFE (Teflon) polymer cell holds two carbons and four atoms of fluorine (Figure 8). All geometrical parameters used in the calculations were taken from experimental X-ray data.⁴⁵ The calculated isotropic values for the ¹⁹F chemical shifts with respect to F₂ are listed in Table 8. Also displayed are ADF results from a calculation on a molecular cluster, F-(CF₂)₂₈-F as well as experimental findings. The BAND calculations afford a ¹⁹F isotropic shift of -585.8 ppm. Convergence was reached with three **k**-points and three primitive cells in a supercell. For the ADF cluster calculation, we have obtained a ¹⁹F shielding constant of -588.1 ppm, and the experimental value is -549 ppm. It seems that DFT in this case falls somewhat short of experiment.

Poly(vinylidene fluoride). The PVDF polymer has two atoms each of carbon, hydrogen, and fluorine in one unit cell (Figure 9). All the structural data used in the calculations were based on experimental X-ray data.⁴⁶ We list in Table 8 the value of the ¹⁹F isotropic chemical shifts with respect

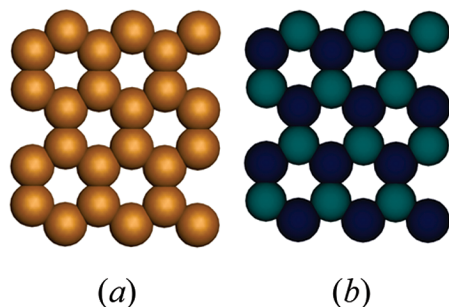


Figure 10. Twenty-four atom square supercell for graphite (a) and boron nitride (b) sheets.

Table 9. ^{13}C Chemical Shift (in ppm) for 2D Graphite with Respect to TMS

	atom probed by NMR	BAND	ADF cluster	calculated by other authors	experiment
2D graphite	C	127.1 ^a	119.2 ^b	118.0 ^c	155,179 ^d

^a BAND calculations with $k\text{space} = 5$ and the supercell with 24 atoms; TZ2P NAO/STO basis. ^b ADF calculations based on a $\text{C}_{188}\text{H}_{38}$ cluster; TZ2P STO basis. ^c From ref 5. ^d From ref 49.

to CFCl_3 from BAND calculations. Comparisons are further given with experimental findings and results from ADF calculations on the molecular cluster $\text{H}-(\text{CH}_2-\text{CF}_2)_9-\text{CH}_3$. For BAND, we reach a converged value of -135.0 ppm with 3 \mathbf{k} -points and 3 primitive units in a supercell. For the ADF cluster calculation, we have obtained a similar value of -133.9 ppm. The experimental estimates contain four different peaks due to structural defects and ranges from 91.6 to 115.6 ppm.⁴⁷

Two- and Three-Dimensional Periodic Systems. Planar

2D graphite has a hexagonal lattice with two atoms in a primitive cell (Figure 10). The C–C bond length is equal to 1.418 Å. We compile the isotropic ^{13}C chemical shift values with respect to TMS from BAND in Table 9. In the same table are given experimental findings as well as ADF results from a calculation on a molecular cluster consisting of 75 benzene rings. The converged BAND result is 127.1 ppm. It was obtained from a square supercell with 24 atoms and $k\text{space} = 5$ (total number 45 of \mathbf{k} -points). For the ADF cluster calculation, we have determined a shielding constant of 119.2 ppm. The experimental values range from 155 to 179 ppm.⁴⁹ It is possible that both theoretical models fall short of the experimental value because DFT at the GGA level used here is unable to describe dispersion. Also we do not consider the Knight shift or the semimetallic behavior exhibited by graphite at low temperatures. Nevertheless, we include our graphite results in order to compare with other implementations where use has been made of the same approximations as here.

Planar 2D boron nitride has a hexagonal lattice with two atoms in a primitive cell with B–N bond length is equal to 1.446 Å. We compile the isotropic ^{15}N chemical shift values with respect to nitromethane from BAND in Table 10. In the same table are given experimental findings as well as ADF results from a calculation on a molecular cluster consisting of 75 BN rings. The converged BAND result is -272.5 ppm. It was obtained from a square supercell with 24 atoms and $k\text{space} = 3$ (total number 15 of \mathbf{k} -points). For

Table 10. ^{15}N Chemical Shift (in ppm) for 2D Boron Nitride with Respect to CH_3-NO_2

	atom probed by NMR	BAND	ADF cluster	calculated by other authors	experiment
2D BN	N	-272.5^a	-264.4^b	-287.0^c	-285^d

^a BAND calculations with $k\text{space} = 3$ and the supercell with 24 atoms; TZ2P NAO/STO basis. ^b ADF calculations based on a $\text{B}_{94}\text{N}_{94}\text{H}_{38}$ cluster; TZ2P STO basis. ^c From ref 50 (cluster consisting of 22 atoms). ^d From ref 50.

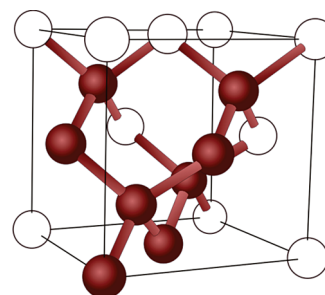


Figure 11. Cubic supercell of diamond with eight atoms.

Table 11. Chemical Shift (in ppm) for Diamond with Respect to TMS

	atom probed by NMR	BAND	calculated by other authors	experiment
diamond	C	35.8 ^a	49.6 ^b 36.17 ^d	34.54 ^c 35.7–38.3 ^e

^a BAND calculations with $k\text{space} = 5$ and the cubic supercell with 8 atoms; TZ2P NAO/STO basis. ^b From ref 4. ^c From ref 51. ^d From ref 52. ^e From ref 53.

the ADF cluster calculation, we have determined a shielding constant of -264.4 ppm. The experimental value for hexagonal boron nitride powder is -285 ppm.

3D crystal of diamond has lattice parameter 3.567 Å. Convergence of the shielding tensor is reached with a 3D \mathbf{k} -space mesh consisting of 123 \mathbf{k} -points ($k\text{space}$ parameter of BAND is equal to 5) and a cubic supercell of 8 atoms (Figure 11). The value calculated by BAND for the ^{13}C isotropic chemical shifts with respect to TMS is listed in Table 11. Also shown are results by other authors and the experimental values. There is in general a good agreement between experiment and theory.

5. Conclusion

We have developed a Kohn–Sham density functional theory (DFT)-based approach for the calculation of NMR shielding tensors in periodic systems. This implementation is gauge-origin invariant. Our implementation differs from others in employing Slater-type or/and numerical atomic orbitals with use of the complete Kohn–Sham potential without recourse to effective potentials. We can thus describe even core orbitals variationally. Integration in the reciprocal space is carried out in one-half of the Brillouin zone. The calculation of NMR chemical shifts for single molecules as well as one-, two- and three-dimensional periodic systems has been used to validate our implementation. Our calculated results agree in most cases with experiment and with results from cluster models and other methods. In our converse procedure, the

calculation of the shielding tensor $\sigma_{\alpha\beta}^N$ for nuclei N requires, first, the evaluation of the current density ΔJ_α induced by the three components ($\alpha = 1, 3$) of the nuclear magnetic moment μ_N , followed by the response of ΔJ_β to the three components ($\beta = 1, 3$) of the external magnetic field \mathbf{B} . When use is made of functionals without current density dependence, the work needed to evaluate $\sigma_{\alpha\beta}^N$ by the converse method is exactly the same as in traditional approaches, where the order of the perturbations has been reversed. This is so since no change in density is induced by either of the magnetic perturbations \mathbf{B} or μ_N . Thus no iterative set of coupled equations is required to be solved, and a direct expression for $\sigma_{\alpha\beta}^N$ can be given that does not depend on the order in which the perturbations are applied. The evaluation of ΔJ_α by a noniterative finite difference procedure rather than analytical differentiation might add some cost. We do not yet have sufficient data to assess the relative merits of periodic NMR calculations compared to those of cluster approaches. However, the use of similar basis sets in both techniques will ultimately allow us to make a valid comparison. For systems with large band gaps, one can employ small supercells, while for systems with a small or vanishing band gap, it is necessary to make use of much larger supercells. The full variational approach taken here lends itself readily to calculation on heavier nuclei, and this will be the subject of a forthcoming investigation.

Acknowledgment. T.Z. would like to thank the Canadian government for a Canada Research Chair in Theoretical Inorganic Chemistry and the NSERC for financial support. We would like to thank Dr. Pier Philipsen for technical help and Dr. Georg Schreckenbach for discussions.

References

- Zurek, E.; Autschbach, J. *Int. J. Quantum Chem.* **2009**, *109*, 3343–3367.
- Mauri, F.; Pfrommer, B. G.; Louie, S. G. *Phys. Rev. Lett.* **1996**, *77*, 5300–5303.
- Pickard, C. J.; Mauri, F. *Phys. Rev. B: Condens. Matter Mater. Phys.* **2001**, *63*, 245101–245113.
- Thonhauser, T.; Ceresoli, D.; Mostofi, A. A.; Marzari, N.; Resta, R.; Vanderbilt, D. *J. Chem. Phys.* **2009**, *131*, 101101; arxiv.org:0709.4429v2.
- Thonhauser, T.; Ceresoli, D.; Marzari, N. *Int. J. Quantum Chem.* **2009**, *109*, 3336–3342.
- Sebastiani, D.; Parinello, M. *J. Phys. Chem. A* **2001**, *105*, 1951–1958.
- Keith, T. A.; Bader, R. F. W. *Chem. Phys. Lett.* **1993**, *210* (1–3), 223–231.
- te Velde, G.; Baerends, E. J. *Phys. Rev. B: Condens. Matter Mater. Phys.* **1991**, *44*, 7888–7903.
- Wiesenecker, G.; te Velde, G.; Baerends, E. J. *J. Phys. C: Solid State Phys* **1988**, *21*, 4263–4283.
- Wiesenecker, G.; Baerends, E. J. *J. Phys.: Condens. Matter* **1991**, *3*, 6721–6742.
- te Velde, G.; Baerends, E. J.; Philipsen, P. H. T.; Wiesenecker, G.; Groeneveld, J. A.; Berger, J. A.; de Boeij, P. L.; Klooster, R.; Kootstra, F.; Romaniello, P.; Snijders, J. G.; Kadantsev, E. S.; Ziegler, T. *BAND*, 2009.01, *SCM: Theoretical Chemistry*, Vrije Universiteit: Amsterdam, The Netherlands; <http://www.scm.com/>.
- Kadantsev, E. S.; Ziegler, T. *J. Phys. Chem. A* **2008**, *112*, 4521–4526.
- Kadantsev, E. S.; Ziegler, T. *J. Phys. Chem. A* **2009**, *113*, 1327–1334.
- Kohn, W.; Sham, L. J. *Phys. Rev.* **1965**, *140*, A1133–A1138.
- McWeeny, R. *Methods of molecular quantum mechanics*; Academic Press: San Diego, 1992.
- te Velde, G. PhD Thesis. Vrije Universiteit: Amsterdam, The Netherlands, 1990; (available on-line: http://www.scm.com/Doc/BAND_thesis/BAND_Thesis.pdf).
- Ditchfield, R. *Mol. Phys.* **1974**, *27* (4), 789–807.
- Gauss, J. Molecular properties. In *Modern methods and algorithms of quantum chemistry, Proceedings*; Grotendorst, J., Ed.; John von Neumann Institute for Computing, Jülich, NIC series, 2000, *3*, 541–592.
- Jones, R. O. Introduction to density functional theory and exchange-correlation energy functionals. In *Computational Nanoscience: Do It Yourself!*; Grotendorst, J., Blügel, S., Marx, D., Eds.; John von Neumann Institute for Computing, Jülich, Germany, 2006, *31*, 45–70.
- Pople, J. A.; Krishnan, R.; Schlegel, H. B.; Binkley, J. S. *Int. J. Quantum Chem., Quantum Chem. Symp.* **1971**, *13*, 225–241.
- Kaxiras, E. *Atomic and electronic structure of solids*. Cambridge University Press: New York, NY, 2003.
- Fukui, H. *Magn. Reson. Rev.* **1987**, *11*, 205–274.
- Martin, R. M. *Electronic structure. Basic theory and practical methods*; Cambridge University Press: Cambridge, England, 2004.
- Amos, A. T.; Musher, J. I. *Mol. Phys.* **1967**, *13*, 509–515.
- Resta, R.; Ceresoli, D.; Thonhauser, T.; Vanderbilt, D. *ChemPhysChem* **2005**, *6*, 1815–1819. Thonhauser, T.; Ceresoli, D.; Vanderbilt, D.; Resta, R. *Phys. Rev. Lett.* **2005**, *95*, 137205–137214. Ceresoli, D.; Thonhauser, T.; Vanderbilt, D.; Resta, R. *Phys. Rev. B: Condens. Matter Mater. Phys.* **2006**, *74*, 024408–024413. Xiao, D.; Shi, J.; Niu, Q. *Phys. Rev. Lett.* **2005**, *95*, 137204–137214. Shi, J.; Vignale, G.; Xiao, D.; Niu, Q. *Phys. Rev. Lett.* **2007**, *99*, 197202–197206.
- Thonhauser, T.; Mostofi, A. A.; Marzari, N.; Resta, R.; Vanderbilt, D. arxiv.org:0709.4429v1.
- Mauri, F.; Louie, S. G. *Phys. Rev. Lett.* **1996**, *76*, 4246–4249.
- Becke, A. D. *Phys. Rev. A: At., Mol., Opt. Phys.* **1988**, *38*, 3098–3100.
- Perdew, J. P. *Phys. Rev. B: Condens. Matter Mater. Phys.* **1986**, *33*, 8822–8824.
- Perdew, J. P. *Phys. Rev. B: Condens. Matter Mater. Phys.* **1986**, *34*, 7406.

- (31) Baerends, E. J.; Autschbach, J.; Bashford, D.; Bérces, A.; Bickelhaupt, F. M.; Bo, C.; Boerrigter, P. M.; Cavallo, L.; Chong, D. P.; Deng, L.; Dickson, R. M.; Ellis, D. E.; van Faassen, M.; Fan, L.; Fischer, T. H.; Fonseca Guerra, C.; Ghysels, A.; Giammona, A.; van Gisbergen, S. J. A.; Götz, A. W.; Groeneveld, J. A.; Gritsenko, O. V.; Grüning, M.; Harris, F. E.; van den Hoek, P.; Jacob, C. R.; Jacobsen, H.; Jensen, L.; van Kessel, G.; Kootstra, F.; Krykunov, M. V.; van Lenthe, E.; McCormack, D. A.; Michalak, A.; Mitoraj, M.; Neugebauer, J.; Nicu, V. P.; Noodleman, L.; Osinga, V. P.; Patchkovskii, S.; Philipsen, P. H. T.; Post, D.; Pye, C. C.; Ravenek, W.; Rodríguez, J. I.; Ros, P.; Schipper, P. R. T.; Schreckenbach, G.; Seth, M.; Snijders, J. G.; Solà, M.; Swart, M.; Swerhone, D.; te Velde, G.; Vernooijs, P.; Versluis, L.; Visscher, L.; Visser, O.; Wang, F.; Wesolowski, T. A.; van Wezenbeek, E. M.; Wiesenekker, G.; Wolff, S. K.; Woo, T. K.; Yakovlev, A. L.; Ziegler, T. *ADF*, 2009.01; SCM: Theoretical Chemistry; Vrije Universiteit: Amsterdam, The Netherlands, 2009.
- (32) te Velde, G.; Bickelhaupt, F. M.; van Gisbergen, S. J. A.; Fonseca Guerra, C.; Baerends, E. J.; Snijders, J. G.; Ziegler, T. *J. Comput. Chem.* **2001**, 22, 931–967.
- (33) Schreckenbach, G.; Ziegler, T. *J. Phys. Chem.* **1995**, 99, 606–611.
- (34) Schreckenbach, G.; Ziegler, T. *Int. J. Quantum Chem.* **1996**, 60, 753–766.
- (35) Computational chemistry comparison and benchmark database; National Institute of Standards and Technology: Gaithersburg, MD; <http://cccbdb.nist.gov/>. Accessed 2005.
- (36) Caminiti, R.; Pandolfi, L.; Ballirano, P. *J. Macromol. Sci.* **2000**, B39 (4), 481–492.
- (37) Yamanobe, T.; Sorita, T.; Comoto, T.; Ando, I. *J. Mol. Struct.* **1985**, 131, 267–275.
- (38) Yamanobe, T. Structure and dynamics of crystalline and noncrystalline phases in polymers. In *Solid State NMR of Polymers*; Ando, I., Ed.; Elsevier & Technology Books: Amsterdam, The Netherlands, 1998, pp 267–1306.
- (39) Perego, G.; Luglia, G.; Pedretti, U.; Cesari, M. *Makromol. Chem.* **1988**, 189, 2657–2669.
- (40) Terao, T.; Maeda, S.; Yamabe, T.; Akagi, K.; Shirakawa, H. *Chem. Phys. Lett.* **1984**, 103 (5), 347–351.
- (41) Tabor, B. J.; Magre, E. P.; Boon, J. *Eur. Polym. J.* **1971**, 7, 1127–1133.
- (42) Napolitano, R.; Pirozzi, B.; Salvione, A. *Macromolecules* **1999**, 32, 7682–7687.
- (43) Wade, B.; Abhiraman, A. S.; Wharry, S.; Sutherlin, D. *J. Polym. Sci.* **1990**, B28, 1233–1249.
- (44) Lowman, D. W.; Fagerburg, D. R. *Bull. Magn. Reson.* **1992**, 14 (1–4), 148–152.
- (45) Iwasaki, M. *J. Polym. Sci., Part A: Polym. Chem.* **2003**, 1 (4), 1099–1104.
- (46) Hasegawa, R.; Takanashi, Y.; Chatani, Y.; Tadokoro, H. *Polym. J. (Tokyo)* **1972**, 3 (5), 600–610.
- (47) Tonelli, A. E.; Schilling, F. C.; Cais, R. E. *Macromolecules* **1982**, 15, 849–853.
- (48) Gabuda, S. P.; Kozlova, S. G.; Paasonen, V. M.; Nazarov, A. S. *J. Struct. Chem.* **2000**, 41 (1), 67–71.
- (49) Sagunama, M.; Mizutami, U.; Kondow, T. *Phys. Rev. B: Condens. Matter Mater. Phys.* **1980**, 22, 5079–5084.
- (50) Marian, C. M.; Gastreich, M. *Solid State Nucl. Magn. Reson.* **2001**, 19, 29–44.
- (51) Merwin, L. H.; Johnson, C. E.; Weimer, W. A. *J. Mater. Res.* **1994**, 9 (3), 631–635.
- (52) Mauri, F.; Pfrommer, B. G.; Louie, S. G. *Phys. Rev. Lett.* **1997**, 79 (12), 2340–2343.
- (53) Alam, T. M. *Mater. Chem. Phys.* **2004**, 85, 310–315.

CT100046A